




On the size of superconducting islands on the density-wave background in organic metals

Vladislav D. Kochev¹, Seidali S. Seidov¹, Pavel .D. Grigoriev^{2,1*}

¹ National University of Science and Technology "MISiS", 119049, Moscow, Russia

² L.D. Landau Institute for Theoretical Physics, 142432 Chernogolovka, Russia

* Correspondence: grigorev@itp.ac.ru

Abstract: Most high- T_c superconductors are spatially inhomogeneous. Usually, this heterogeneity originates from the interplay of various types of electronic ordering. It affects various superconducting properties, such as the transition temperature, magnetic upper critical field, critical current, etc. In this paper we analyze the parameters of spatial phase segregation during the first-order transition between superconductivity (SC) and a charge- or spin-density wave state in quasi-one-dimensional metals with imperfect nesting, typical to organic superconductors. An external pressure or another driving parameter increases the transfer integrals in electron dispersion, which only slightly affects SC but violates the Fermi-surface nesting and suppresses the density wave (DW). At a critical pressure P_c the transition from DW to SC occurs. We estimate the characteristic size of SC islands during this phase transition in organic metals in two ways. Using the Ginzburg-Landau expansion we analytically obtain a lower bound for the size of SC domains. To estimate more specific interval of possible size of the SC islands in (TMTSF)₂PF₆ samples we perform numerical calculations of the percolation probability via SC domains and compare it with experimental resistivity data. This helps to develop a consistent microscopic description of SC spatial heterogeneity in various organic superconductors.

Keywords: superconductivity, CDW, charge-density waves, SDW, spin-density wave, phase diagram, organic superconductor

1. Introduction

Superconductivity (SC) often competes [1–3] with charge-density-wave (CDW) or spin-density-wave (SDW) electronic instabilities [3,4], as both create an energy gap on the Fermi level. In such materials the density wave (DW) is suppressed by some external parameter, which deteriorates the nesting property of Fermi surface (FS) and enables superconductivity. These driving parameters are, usually, the chemical composition (doping level) and pressure, as in cuprate [5–10] or iron based high- T_c superconductors [11,12], organic superconductors (OS) [13–26], transition metal dichalcogenides [1–3], etc. The DW can also be suppressed [27] or enhanced [28,29] by disorder. The latter happens, e.g., in (TMTSF)₂ClO₄ organic superconductor [13,14,28–30], where the disorder is controlled by cooling rate during the anion ordering transition. The anion ordering splits the electron spectrum, which deteriorates the FS nesting and damps SDW, enabling SC.

The SC-DW interplay is much more interesting than just a competition. Usually, the SC transition temperature T_c is the highest in the coexistence region near the quantum critical point where DW disappears [20,21,31,32]. It is attributed to the enhancement of Cooper pairing by the critical DW fluctuations, similar to cuprate high- T_c superconductors [33], and is also common for other types of quantum critical point [34,35]. The enhancement of electron-electron (e - e) interaction in the Cooper channel appears already in the random-phase approximation, and the resulting strong momentum dependence of e - e coupling may lead to unconventional superconductivity [36]. The upper critical field H_{c2} is often several times higher in the coexistence region than in a pure SC phase [18,25], which may be useful for applications.

The OS are helpful for investigating the SC-DW interplay because they have rather weak electronic correlations and low DW and SC transitions temperatures [13,14], which is convenient for their theoretical and experimental study. However, their phase diagram, layered crystal structure and many other features are very similar to those in high- T_c superconductors. Moreover, by changing the chemical composition or pressure in OS, one can easily vary the electronic dispersion in a wide interval and even change the FS topology from quasi-1D (Q1D) to quasi-2D. Large and pure monocrystals of organic metals can be synthesized, so that their electronic structure can be experimentally studied by high-magnetic-field tools [37] and by other experimental techniques [13,14].

To understand the DW-SC interplay and the influence of DW on SC properties in OS one needs to know the microscopic structure of their coexistence. Each of these ground states creates an energy gap on the Fermi level and removes the FS instability. Hence, the DW and SC must be somehow separated in the momentum or coordinate space. The momentum-space DW-SC separation assumes a spatially uniform structure, where the FS is only partially gapped by DW, and the ungapped parts of FS hold SC [3,38]. The resistivity hysteresis observed in (TMTSF)₂PF₆ [19] suggests the spatial DW/SC segregation in OS. The microscopic SC domains of size d comparable to the DW coherence length ξ_{DW} may emerge due to the soliton DW structure [39–43]. However, such a small size of SC or metallic domains contradicts the angular magnetoresistance oscillations (AMRO) in the region of SC/DW coexistence, observed both in (TMTSF)₂ClO₄ [30] and in (TMTSF)₂PF₆ [21] and implying the domain width $d > 1 \mu\text{m}$ [21,30].

The observed [18,25] enhancement of SC upper critical field H_{c2} in OS is possible in all of the above scenarios [38,41]. For spatial DW-SC segregation it only requires the SC domain size being of the order of the penetration depth λ of magnetic field to the superconductor [44]. In (TMTSF)₂ClO₄ the penetration depth within the TMTSF layers is [45] $\lambda_{ab}(T = 0) \approx 0.86 \mu\text{m}$ and increases with $T \rightarrow T_{c\text{SC}}$. Hence, the macroscopic spatial phase separation with SC domain size $d > 1 \mu\text{m}$ suggested by AMRO data [21,30] is consistent with the observed H_{c2} enhancement in the DW-SC coexistence phase.

Another interesting feature of SDW/SC coexistence in OS is the anisotropic SC onset, opposite to a weak intrinsic interlayer Josephson coupling in high- T_c superconductors [44]: the SC transition and the zero resistance in OS is first observed [20,21,28] only along the least-conducting interlayer z -direction, then along two least-conducting directions, z and y , and only finally in all three directions. This anisotropic SC onset was explained recently [46] by assuming a spatial SC/DW separation and studying the percolation in finite-size samples of the thin elongated shape, relevant to the experiments in (TMTSF)₂PF₆ [20,21] and (TMTSF)₂ClO₄ [28,29]. This additionally supports the scenario of spatial SC/DW segregation in a form of rather large domains of width $d > 1 \mu\text{m}$. However, the microscopic reason for such phase segregation remains unknown. Similar anisotropic SC onset and even T_c enhancement in FeSe mesa structures was observed and explained by heterogeneous SC inception [47]. The spatial segregation in FeSe and some other Fe-based high- T_c superconductors, probably, originates from the so-called nematic phase transition and domain structure, but similar electronic ordering is absent in OS.

Recently, the DW-metal phase transition in OS was shown to be of first order [48], which suggests that the spatial DW-SC segregation may be due to the phase nucleation during this transition. In this paper we estimate the typical size of SC islands in organic metals with two different methods. In Sec. 2 we formulate the model and write down the Landau-Ginzburg functional for free energy in the DW state. In Sec. 3.1 we analytically obtain a lower bound for the size of the SC islands. In Section 3.2, we discuss the relationship between the DW coherence length and the SC nucleation size during the first-order phase transition. In Sec. 3.3 we perform numerical calculations of the percolation probability from which we conclude about the interval of possible sizes of the SC islands in (TMTSF)₂PF₆. In Sec. 4 we discuss our results in connection with the experimental observations in (TMTSF)₂PF₆ and in other superconductors.

2. The model

2.1. Q1D electron dispersion and the driving parameter of DW-metal/SC phase transition in OS

In Q1D organic metals [13,14] the free electron dispersion near the Fermi level is approximately given by

$$\varepsilon(\mathbf{k}) = \hbar v_F(|k_x| - k_F) + t_{\perp}(\mathbf{k}_{\perp}), \quad (1)$$

where v_F and k_F are the Fermi velocity and Fermi momentum in the chain (x) direction. The interchain electron dispersion $t_{\perp}(\mathbf{k}_{\perp})$ is given by the tight-binding model:

$$t_{\perp}(\mathbf{k}_{\perp}) = -2t_b \cos(k_y b) - 2t'_b \cos(2k_y b), \quad (2)$$

where b is the lattice constants in the y -direction. Because the dispersion along the interlayer z -axis is usually significantly less than along the y -axis, it is left out here. In (TMTSF)₂PF₆ the transfer integral $t_b \approx 30 \text{ meV}$ [49], and the “ant nesting” parameter $t'_b \approx 4.5 \text{ K}$ [50] at ambient pressure.

As illustrated in Fig. 1b, the FS of Q1D metals consists of two slightly warped sheets separated by $2k_F$ and roughly exhibits the nesting property. It leads to the Peierls instability and favors the formation of DW at low temperature $T < T_{\text{cDW}} \equiv T_c$, which competes with superconductivity. The quasiparticle dispersion in the DW state in the mean-field approximation is given by

$$E_{\pm}(\mathbf{k}) = \varepsilon_{+}(\mathbf{k}, \mathbf{k} - \mathbf{Q}) \pm \sqrt{|\Delta_{\mathbf{Q}}|^2 + \varepsilon_{-}^2(\mathbf{k}, \mathbf{k} - \mathbf{Q})}, \quad (3)$$

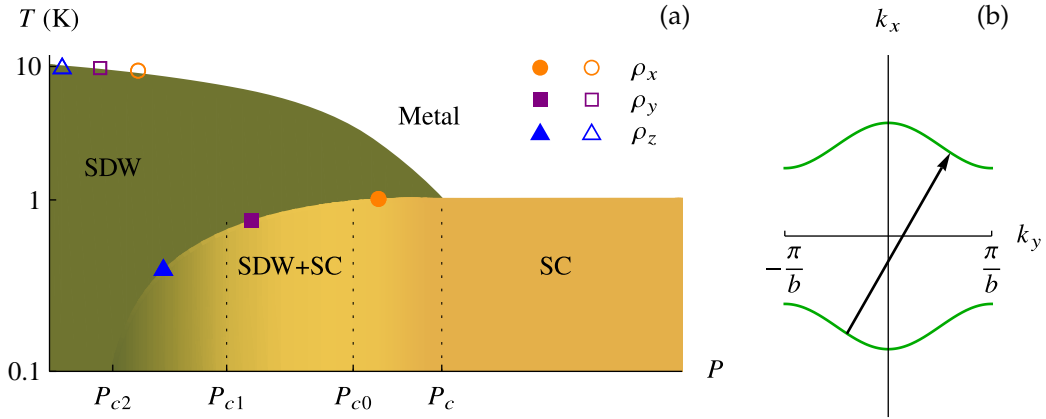


Figure 1. (a) Pressure-temperature phase diagram of (TMTSF)₂PF₆ recreated from resistivity data in Ref. [20]; (b) schematic Fermi surface of (TMTSF)₂PF₆, obtained from the quasi-1D electron dispersion given by Eqs. (1) and (2). The nesting vector Q is indicated by the black arrow.

where we have used the notations

$$\varepsilon_{\pm}(k, k') = \frac{\varepsilon(k) \pm \varepsilon(k')}{2}. \quad (4)$$

The FS has the property of perfect nesting at the wave vector Q if $\varepsilon_+(k, k - Q) = 0$. If $\varepsilon_+(k, k - Q) < |\Delta_Q|$ for the entire FS, all electron states are gapped at the Fermi level due to the DW formation. Then the DW results to a semiconducting state at $T < T_{\text{CDW}}$ and SC does not appear. If $\varepsilon_+(k, k - Q) > |\Delta_Q|$ in a finite interval of k at the Fermi level, the metallic state survives at $T < T_{\text{CDW}}$. Then a uniform SC state may appear, but its properties differ from those without DW [38,43] because of the FS reconstruction and the change of electron dispersion by the DW. For $Q = Q_0 = (2k_F, \pi/b)$ only the second harmonic in the electron dispersion given by Eq. (2) violates the FS nesting: $\varepsilon_+(k, k - Q_0) = -2t'_b \cos(2k_y b)$. Hence, usually, only $t'_b \sim t'_b / v_F k_F \ll t_b$ is important for the DW phase diagram.

With the increase of applied pressure P the lattice constants decrease. This enhances the interchain electron tunneling and the transfer integrals. The increase of $t'_b(P)$ with pressure spoils the FS nesting and decreases the DW transition temperature $T_{\text{CDW}}(P)$. There is a critical pressure P_c and the corresponding critical value $t'^*_b = t'_b(P_c)$ at which $T_{\text{CDW}}(P_c) = 0$ and one has a quantum critical point (QCP). The electronic properties at this DW QCP are additionally complicated by superconductivity emerging at $T < T_{\text{SC}}$ at $P > P_c$. In organic metals SC appears even earlier, at $P > P_{c1} < P_c$, and there is a finite region $P_{c1} < P < P_c$ of SC-DW coexistence [20,21,25]. This simple model qualitatively describes the phase diagram observed in (TMTSF)₂PF₆ [20,21,25], α -(BEDT-TTF)₂KHg(SCN)₄ [25], in various compounds of (TMTTF)₂X family [26,51,52] and in many other OS [13,14,16,17].

2.2. Mean field approach and the Landau-Ginzburg expansion of DW free energy

The mean-field theory does not describe correctly the strictly 1D conductors, where the non-perturbative methods are helpful. However, in most DW materials the nonzero electron hopping between the conducting 1D chains and the 3D character of the electron-electron (e-e) interactions and lattice elasticity reduce the deviations from the mean-field solution and also make most of the methods and exactly solvable models developed for strictly 1D case inapplicable. On the other hand, the interchain electron dispersion strongly damps the fluctuations and validates the mean-field description [53,54]. The perpendicular-to-chain term $t_{\perp}(k_{\perp})$ in Eqs. (1) and (2) is much greater than the energy scale of the DW transition temperature, $T_{c0} \approx 12.1$ K. Only the "imperfect nesting" term $\sim t'_b$ of $t_{\perp}(k_{\perp})$ is of the order of T_{c0} . Hence, the criterion for the mean-field theory to be applicable [53,54] $t_{\perp} \gg T_{c0}$, is reliably satisfied in most Q1D organic metals.

For our analysis we take the Landau-Ginzburg expansion of the free energy in the series of even powers of DW order parameter $\Delta = \Delta_Q$:

$$F \simeq \frac{A(T, Q)}{2} |\Delta|^2 + \frac{B}{4} |\Delta|^4 + \frac{C}{6} |\Delta|^6 + \frac{D}{8} |\Delta|^8 + \dots \quad (5)$$

Usually, the minimum of the free energy corresponds to the uniform DW order parameter Δ , when $Q = Q_0$. Since the coefficient $A(T_{\text{CDW}}, Q_0) = 0$, we keep its temperature and momentum dependence. The sign of the coefficient B determines the type of DW-metal phase transition. If $B_{\text{DW}} > 0$, the phase transition is of the second order, and only the first two coefficients A_{DW} and B_{DW} are sufficient for its description. If $B_{\text{DW}} < 0$, the phase transition may be of the first

order, and next coefficients C_{DW} and even D_{DW} if $C_{DW} \leq 0$ are required for its description. The self-consistency equation (SCE) for a DW is obtained by the variation of the free energy (5) with respect to Δ :

$$\Delta \left(A + B|\Delta|^2 + C|\Delta|^4 + D|\Delta|^6 + \dots \right) = 0. \quad (6)$$

The free energy (5) can also be calculated by integrating the SCE over Δ . In Ref. [55] the SCE for the DW was derived in a magnetic field acting via Zeeman splitting and for two coupling constants of e - e interaction, charge U_c and spin U_s (see Eqs. (17) in Ref. [55]). Without magnetic field the charge U_c and spin U_s coupling constants do not couple, and the system chooses only one of them, the largest one, corresponding to the highest transition temperature. We rewrite this SCE without magnetic field and for only one charge or spin coupling constant U :

$$\Delta = -TU \sum_{k\omega} \frac{\Delta}{(\omega + i\varepsilon_+)^2 + \varepsilon_-^2 + |\Delta|^2}, \quad (7)$$

where $\varepsilon_{\pm} = \varepsilon_{\pm}(\mathbf{k}, \mathbf{k} - \mathbf{Q})$ are given by Eq. (4), and ω takes the values $\pi T(2n + 1)$, $n \in \mathbb{Z}$. In Appendix A we briefly describe the derivation of Eq. (7) and discuss the relation of coefficients in Landau-Ginzburg expansion (5) with electronic susceptibility. The Landau-Ginzburg expansion coefficients in Eqs. (5) and (6) can be obtained by the expansion of Eq. (7) in a power series of $|\Delta|^2$.

The sum over \mathbf{k} in Eq. (7) for macroscopic sample is equivalent to the integral

$$\sum_{\mathbf{k}} = 2 \int \frac{dk_x}{2\pi} \int_{-\pi/b}^{\pi/b} \frac{dk_y}{2\pi}. \quad (8)$$

The factor 2 appears because of two FS sheets at $k_x \approx \pm k_F$. Usually, for simplicity the integration limits over k_x are taken to be infinite, and the resulting logarithmic divergence of Eq. (7) is regularized by the definition of the transition temperature T_{c0} . This procedure is briefly described in Appendix B of Ref. [48]. When the Fermi energy $E_F \gg t_b$, for a linearized electron dispersion (1) near the Fermi level one may integrate Eq. (7) over k_x in infinite limits, which gives (cf. Eq. (22) of Ref. [55])

$$\Delta = \frac{\pi v_F |U| T}{2} \sum_{\omega} \left\langle \frac{\Delta}{\sqrt{(\omega + i\varepsilon_+)^2 + |\Delta|^2}} \right\rangle_{k_y}, \quad (9)$$

where the density of electron states at the Fermi level in the metallic phase per two spin components per unit length L_x of one chain is $\nu_F = 2/\pi\hbar v_F$. Averaging over k_y is denoted by triangular brackets, i.e. $\langle \bullet \rangle_{k_y} = b \int_{-\pi/b}^{\pi/b} dk_y / 2\pi$. Eq. (9) is similar to the self-consistency equation for superconductivity in magnetic field, where the orbital effect of magnetic field is neglected and the pair-breaking Zeeman splittig is replaced by $\varepsilon_+(\mathbf{k}, \mathbf{k} - \mathbf{Q})$.

3. Estimation of size of the SC islands

3.1. Analytical calculation of the Ginzburg-Landau expansion coefficients for $T \gg t_b'$

Expansion of Eq. (9) over Δ yields

$$A = -\frac{4\pi T}{\hbar v_F} \sum_{\omega} \left\langle \frac{\text{sgn } \omega}{\omega + i\varepsilon_+} \right\rangle_{k_y} - \frac{1}{U} = -\frac{4}{\hbar v_F} \left[\ln \frac{T_{c0}}{T} + \psi\left(\frac{1}{2}\right) - \left\langle \text{Re } \psi\left(\frac{1}{2} + \frac{\varepsilon_+}{2\pi T}\right) \right\rangle_{k_y} \right], \quad (10)$$

where the logarithmic divergence $\pi T \sum_{\omega} |\omega|^{-1} \approx \ln(E_F/T)$ is contained in the definition of $T_{c0} = E_F \exp\{-1/(v_F |U|)\}$. In (TMTSF)₂PF₆ $T_{c0} \approx 12.1$ K [50].

The spatial modulation with wave vector \mathbf{q} of the DW order parameter Δ corresponds to the deviation of the DW wave vector \mathbf{Q} from \mathbf{Q}_0 by $\pm \mathbf{q}$. Hence, the gradient term in the Ginzburg-Landau expansion of DW free energy can be obtained by the expansion of $A(T, \mathbf{Q})$ given by Eq. (10) in the powers of small deviation $\mathbf{q} = \mathbf{Q} - \mathbf{Q}_0$. $A(\mathbf{Q}, T)$ depends on \mathbf{Q} via $\varepsilon_+ = \varepsilon_+(\mathbf{k}, \mathbf{k} - \mathbf{Q})$, given by Eq. (4). For the quasi-1D electron dispersion in Eqs. (1) and (2), approximately describing (TMTSF)₂PF₆, we may use Eq. (21) from Ref. [55]:

$$\varepsilon_+ = \frac{\hbar v_F q_x}{2} + 2t_b \sin \frac{b q_y}{2} \sin \left(b \left[k_y - \frac{q_y}{2} \right] \right) - 2t'_b \cos(b q_y) \cos(b [2k_y - q_y]). \quad (11)$$

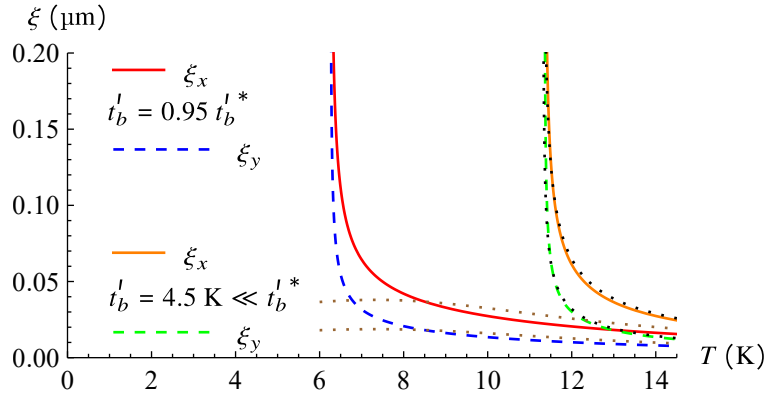


Figure 2. Temperature dependence of DW coherence length ξ along two main axes at two different values of $t'_b = 4.5 \text{ K} = 0.42 t'_b^*$, corresponding to (TMTSF)₂PF₆ at ambient pressure, and at $t'_b = 0.95 t'_b^*$. Solid and dashed lines correspond to the numerical solution of the Eqs. (14), while the dotted lines correspond to the approximate analytical formulas in Eqs. (17) and (18).

The general form of the Taylor series of $A(T, \mathbf{Q}_0 + \mathbf{q})$ given by Eq. (10) over the deviation $\mathbf{q} = \mathbf{Q} - \mathbf{Q}_0$ of the DW wave vector \mathbf{Q} from its optimal value \mathbf{Q}_0 up to the second order is

$$A(\mathbf{q}) \simeq -\frac{4}{\hbar v_F} \left[\ln \frac{T_{c0}}{T} + \int_{-\pi/b}^{\pi/b} dk_y \left(C_0 + c_x q_x + c_y q_y + c_{xy} q_x q_y + A_x q_x^2 + A_y q_y^2 \right) \right]. \quad (12)$$

The linear terms and the cross term vanish when taking the integral $\int_{-\pi/b}^{\pi/b} dq_y$ (this is always the case if wave vector \mathbf{Q}_0 is the optimal one). The constant and quadratic terms do not vanish, hereby

$$A(\mathbf{q}) \simeq A_0 + A_x q_x^2 + A_y q_y^2. \quad (13)$$

Expanding Eq. (11) over the deviation $\mathbf{q} = \mathbf{Q} - \mathbf{Q}_0$ up to the second order, substituting it in Eq. (10) and expanding the digamma function over the same wave vector \mathbf{q} , we obtain the coefficients A_i :

$$\begin{aligned} A_0 &= -\frac{4}{\hbar v_F} \left[\frac{T_{c0}}{T} + \psi\left(\frac{1}{2}\right) - \left\langle \text{Re} \psi\left(\frac{1}{2} - \frac{it'_b \cos(2bk_y)}{\pi T}\right) \right\rangle_{k_y} \right]; \\ A_x &= -\frac{4}{\hbar v_F} \frac{\hbar^2 v_F^2}{32\pi^2 T^2} \left\langle \text{Re} \psi^{(2)}\left(\frac{1}{2} - \frac{it'_b \cos(2bk_y)}{\pi T}\right) \right\rangle_{k_y}; \\ A_y &= \frac{4}{\hbar v_F} \frac{b^2}{8\pi^2 T^2} \left\langle 2\pi T [t_b \cos(bk_y) - 4t'_b \cos(2bk_y)] \text{Im} \psi^{(1)}\left(\frac{1}{2} - \frac{it'_b \cos(2bk_y)}{\pi T}\right) - \right. \\ &\quad \left. - [t_b - 4t'_b \cos(bk_y)]^2 \sin^2(bk_y) \text{Re} \psi^{(2)}\left(\frac{1}{2} - \frac{it'_b \cos(2bk_y)}{\pi T}\right) \right\rangle_{k_y}. \end{aligned} \quad (14)$$

The integrals A_y , A_x and A_0 can be calculated numerically and give the coherence lengths ξ_x and ξ_y . From Eqs. (A10) and (A11) it follows that

$$\xi_i^2 = A_i / A_0. \quad (15)$$

Fig. 2 shows ξ_x and ξ_y as a function of temperature T for two different values of t'_b : $t'_b \approx 0.42 t'_b^*$, corresponding to (TMTSF)₂PF₆ at ambient pressure [50] (solid orange and dashed green lines), and at $t'_b = 0.95 t'_b^*$ (solid red and dashed blue lines), i.e. close to the quantum critical point at $t'_b = t'_b^*$. These curves diverge at $T = T_c(t'_b)$, where $A_0 = 0$. This divergence, being a general property of phase transitions, is well-known in superconductors. For plotting Fig. 2 we used Eqs. (14) and (15), and the parameters of (TMTSF)₂PF₆: $b = 0.767 \text{ nm}$ [56] and $v_F = 10^7 \text{ cm/s}$ [49].

At rather high temperature $2\pi T \gg \varepsilon_+ \sim t_b'$ we may expand the digamma function in Eq. (10) in a Taylor series near the $1/2$, which gives

$$\psi\left(\frac{1}{2}\right) - \left\langle \operatorname{Re} \psi\left(\frac{1}{2} + \frac{i\varepsilon_+(\mathbf{k}, \mathbf{k} - \mathbf{Q})}{2\pi T}\right) \right\rangle_{k_y} \simeq \frac{b}{2\pi} \int_{-\pi/b}^{\pi/b} dk_y \frac{\psi^{(2)}(1/2) \varepsilon_+^2(\mathbf{k}, \mathbf{k} - \mathbf{Q})}{8\pi^2 T^2}. \quad (16)$$

Expanding Eq. (11) over the \mathbf{q} up to the second order and substituting it into Eq. (10) after using Eq. (16), we obtain the coefficients A_i :

$$A_0 = -\frac{4}{\hbar v_F} \left[\ln \frac{T_{c0}}{T} + \frac{t_b'^2}{4\pi^2 T^2} \right];$$

$$A_x = -\frac{4}{\hbar v_F} \psi^{(2)}\left(\frac{1}{2}\right) \left[\frac{\hbar^2 v_F^2}{32\pi^2 T^2} \right]; \quad A_y = -\frac{4}{\hbar v_F} \psi^{(2)}\left(\frac{1}{2}\right) \left[\frac{b^2 (t_b^2 - 4t_b'^2)}{16\pi^2 T^2} \right]. \quad (17)$$

Substituting them to Eq. (15) we derive simple analytical formulas for the SDW coherence lengths ξ_x and ξ_y valid at $\pi T \gg t_b'$:

$$\xi_x = \frac{\hbar v_F}{2\sqrt{2}} \sqrt{1 / \left(4\pi^2 T^2 \ln(T_{c0}/T) / \psi^{(2)}(1/2) + t_b'^2 \right)};$$

$$\xi_y = \frac{b}{2} \sqrt{\frac{t_b^2 - 4t_b'^2}{4\pi^2 T^2 \ln(T_{c0}/T) / \psi^{(2)}(1/2) + t_b'^2}}. \quad (18)$$

In this limit $\pi T \gg t_b'$ the ratio of coherent lengths along y - and x -axis does not depend on temperature:

$$\frac{\xi_y}{\xi_x} = \frac{b}{\hbar v_F} \sqrt{2(t_b^2 - 4t_b'^2)} \approx 0.5. \quad (19)$$

The temperature dependence of the coherence lengths ξ_x and ξ_y given by Eq. (18) are shown in Fig. 2 by dotted lines. The black dotted curves in Fig. 2 are obtained from Eq. (18) by substituting $t_b' = 4.5 \text{ K} = 0.42 t_b^*$, corresponding to (TMTSF)₂PF₆ at ambient pressure [50]. These curves coincide with the result of numerical integration in Eqs. (14), which confirms the applicability of Eqs. (17) and (18) at these parameters. From Eq. (18) we obtain $\xi_x \approx 0.06 \mu\text{m}$, $\xi_y \approx 0.03 \mu\text{m}$ at $T = T_{c0} = 12.1 \text{ K}$, corresponding to $T/T_c - 1 \approx 0.075$. However, at $T/T_c - 1 \approx 0.01$ this gives $\xi_x \approx 0.16 \mu\text{m}$ and $\xi_y \approx 0.08 \mu\text{m}$.

3.2. Relation between the coherence length and nucleation size during the first-order phase transition

In spite of an extensively study of phase nucleation process during the first-order phase transition [57–60], its general quantitative description is still missing. The nucleation rate and size may strongly depend on minor factors relevant to a particular system. The DW-metal or DW-SC phase transitions also have peculiarities, such as strong dependence on the details of electron dispersion. Nevertheless, one can roughly estimate the lower limit of nucleus size using the Ginzburg-Landau expansion for DW free energy. The latter gives the energy of a phase nucleus Ω , described by the spatial variation $\Delta(\mathbf{r})$ of the DW order parameter during the first-order phase transition as

$$\Delta F_\Omega \approx \int_\Omega d^3\mathbf{r} \frac{1}{2} \left[A_0 \Delta^2 + \sum_i A_i (\partial_i \Delta)^2 \right] \approx \int_\Omega d^3\mathbf{r} \frac{A_0}{2} \left[\Delta^2 + \sum_i (\xi_i \partial_i \Delta)^2 \right]. \quad (20)$$

If the nucleus size $d_i < 2\xi_i$, the second (always positive) gradient term exceeds the first term, which is energetically unfavorable. Hence, the minimal dimensions of phase nucleation during the first-order phase transition is given by the coherence lengths: $d_i > 2\xi_i$. The latter diverge at the spinodal line $T_c(t_b')$ of the phase transition where $A_0 = 0$, as illustrated in Fig. 2 for our DW system. However, the first-order phase transition starts at a slightly different temperature T_{c1} , while the spinodal line $T_c(t_b')$ corresponds to the instability of one phase. Hence, for the estimates of nucleus size d_i one should take some finite interval $\Delta T = T_{c1} - T_c$, which is determined by the width of first-order phase transition. Unfortunately, the latter is unknown and strongly depends on physical system. In our case, this width ΔT depends on

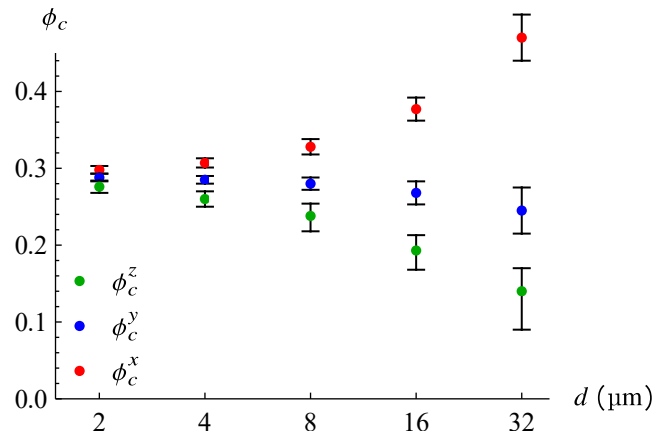


Figure 3. Dependence of the percolation threshold ϕ_c along different axes from the size of the spherical island d in $(\text{TMTSF})_2\text{PF}_6$. The intervals of ϕ_c , corresponding to the percolation probability $p \in (0.5 \pm 0.4)$, are indicated by error bars.

the details of electron dispersion, e.g., on the amplitude of higher harmonics in the electron dispersion given by Eq. (2). If we take a reasonable estimate $\Delta T = T_{c1} - T_c \approx 0.01 T_c$, we obtain the SC domain size $d > 2\xi > 0.3 \mu\text{m}$.

3.3. Estimates of superconducting island size from transport measurements and the numerical calculation of current percolation threshold

Another method of estimating the average SC island size is based on using the available transport measurements, especially the anisotropy of SC transition temperature observed in various organic superconductors [20,21,28] and determined from the anisotropic zero-resistance onset in various samples. This anisotropy was explained both in organic superconductors [46] and in mesa structures of FeSe [47] by the direct calculation of the percolation threshold along different axes in samples of various spatial dimensions relevant to experiments. The qualitative idea behind this anisotropy is very simple. As the volume fraction ϕ of SC phase grows, the isolated clusters of SC islands grow and become comparable to the sample size. When the percolation via SC islands between the opposite sample boundaries establishes, the zero resistance sets in. If the sample shape is flat or needle-like, as in organic metals, this percolation first establishes along the shortest sample dimension, when the SC cluster becomes comparable to the sample thickness (see Fig. 4a of Ref. [46] or Fig. 4b of Ref. [47] for illustration). With the further increase of SC volume fraction ϕ the zero resistance sets in along two axes, and only finally in all three directions, including the sample length.

In the infinitely large samples the percolation threshold is isotropic [61]. Hence, this anisotropy depends on the ratio of average size d of SC islands to the sample size L . This dependence can be used for a qualitative estimate of SC island size d by analyzing the interval of d where the experimental data on conductivity anisotropy are consistent with theoretical calculations.

The algorithm and implementation details of percolation calculations are given in the Refs. [46,47]. Using this method, we calculated the probability of percolation of a random geometric configuration of superconducting islands in a sample of $(\text{TMTSF})_2\text{PF}_6$ with typical experimental dimensions $3 \times 0.2 \times 0.1 \text{ mm}^3$ [19,20] for various island sizes. For simplicity, the geometry of islands was taken spherical.

Fig. 3 shows the dependence of percolation threshold ϕ_c of the SC phase on the geometric dimensions of SC islands. By the percolation threshold we mean the SC volume fraction ϕ at which the probability of percolation of a randomly chosen geometrical configuration of islands is $1/2$. To take into account possible random fluctuations of this SC current percolation, in Fig. 3 we also plot the interval of SC volume fraction ϕ , corresponding to the large interval of percolation probability $p \in (0.1, 0.9)$ and denoted by the error bar. From Fig. 3 we see that for the sample dimensions as in the experiment [20], the percolation threshold via SC domains is considerably anisotropic, beyond the random fluctuations corresponding to particular sample realization, if the domain size exceeds $2 \mu\text{m}$. For smaller size of SC islands the anisotropy is smaller than the “error bar” of ϕ_c , corresponding to the fluctuations of percolation probability $p \in (0.1, 0.9)$. For $d < 2 \mu\text{m}$ the percolation thresholds along all three axes converge to the known isotropic percolation threshold in infinite samples $\phi_{c\infty} \approx 0.2895$ (see page 253 of Ref. [62]).

4. Discussion and conclusion

The observed strong anisotropy of SC transition temperature T_{cSC} in $(\text{TMTSF})_2\text{PF}_6$ [20,21] and $(\text{TMTSF})_2\text{ClO}_4$ [28] samples of thickness $\sim 0.1 \text{ mm}$ is consistent with our percolation calculations if the SC domain size $d > 2 \mu\text{m}$.

These estimates of SC domain size d agree well with the result $d_x > 1 \mu\text{m}$, implied by the clear observation of angular magnetoresistance oscillations and of field-induced spin-density wave in $(\text{TMTSF})_2\text{PF}_6$ [21] and in $(\text{TMTSF})_2\text{ClO}_4$ [30]. The latter requires that the electron mean free path $l_\tau > l_B$, where $l_B = \hbar/eBb \sim 1 \mu\text{m}$ is the so-called quasi-1D magnetic length [21,37]. Hence, all experimental observations agree and suggest almost macroscopic spatial separation of SC and SDW phases in these organic superconductors.

The above SDW coherence length ξ obtained from the Ginzburg-Landau expansion of SDW free energy at the first-order SDW-SC phase transition in the organic superconductor $(\text{TMTSF})_2\text{PF}_6$ gives the SC domain size $d > 2\xi > 0.3 \mu\text{m}$. This generally agrees with the experimental estimates $d > 1 \mu\text{m}$, but gives a too weak limitation because of the following three possible reasons:

- (1) The SC proximity effect [44]: the SC order parameter is nonzero not only in the SC domains themselves, but also in the shell of width $\delta d \sim \xi_{\text{SC}}$ around these SC domains. The SC coherence length $\xi_{\text{SC}} \sim \hbar v_F / \pi \Delta_{\text{SC}}$ diverges near the SC transition temperature T_{cSC} , but even far from $T_{\text{cSC}} \approx 1 \text{ K}$ in organic superconductors $\delta d_x \sim \xi_{\text{SC}} \sim \hbar v_F / \pi T_{\text{cSC}} \approx 0.3 \mu\text{m}$. Hence, the resulting size of SC domains with this proximity-effect shell is $d_x \gtrsim 2(\xi_{\text{SC}} + \xi) \approx 1 \mu\text{m}$, which well agrees with experimental data.
- (2) The clusterization of SC islands with the formation of larger SC domains, glued by the Josephson junction. In current percolation and zero-frequency transport measurements such a cluster is seen as a single SC domain. Since the SDW-SC transition is observed close to SC percolation threshold, the SC volume fraction $\phi_c > 0.1$, and the formation of such SC clusters is very probable. Note that such clusterization may also explain the small difference between the estimates of SC domain size from AMRO data and from current percolation.
- (3) Oversimplified physical model. In our percolation calculations we take all clusters of the same size, because the actual size distribution of SC islands is unknown. In addition, special types of disorder, such as local variations of (chemical) pressure, affect the SC-SDW balance.

The size of isolated SC domains allows an independent approximate measurement from the diamagnetic response. The diamagnetic response of small SC grains of size $d \lesssim \lambda$, where λ is the penetration depth of magnetic field to the superconductor, strongly depends on the ratio d/λ [44]. Note that this penetration depth in layered superconductors is anisotropic. Since the SC volume fraction ϕ is approximately known from the transport measurements and from percolation threshold, by measuring the diamagnetic response at $\phi < \phi_c$ for three main orientations of magnetic field \mathbf{B} and comparing it with the susceptibility $\chi = -\phi/(4\pi)$ of large SC domains of volume fraction ϕ , one may roughly estimate the SC domain size along all three axes. Similar diamagnetic response in combination with transport measurements was used in FeSe to estimate the size and shape of SC islands above T_{cSC} [63,64]. Similar combined analysis of diamagnetic response and transport measurements also gives information about the SC domain size and shape above T_{cSC} in another organic superconductor $\beta\text{-(BEDT-TTF)}_2\text{I}_3$ [65].

The obtained almost macroscopic spatial SDW-SC phase separation on a scale $d \gtrsim 1 \mu\text{m}$ implies a rather weak influence of SDW quantum critical point on the SC coupling. Indeed, while in cuprate high- T_c superconductors [5,33,66–69] and in transition metal dichalcogenides [1–3] the SC-DW coexistence is more “microscopic”, and the corresponding T_{cSC} enhancement is severalfold, in the organic superconductors the T_{cSC} enhancement by quantum criticality is rather weak, $\sim 10\%$. Note that in iron-based high- T_c superconductors [11,12], e.g. in FeSe, the T_{cSC} enhancement by quantum criticality is also rather weak, $\sim 10\%$. The comparison of the observed [47,70] T_{cSC} anisotropy in thin FeSe mesa structures of various thickness with the numerical calculations of percolation anisotropy in finite-size samples [47], similar to that in Sec. 3.3, suggests the SC domain size in FeSe also rather large, $d \sim 0.1 \mu\text{m}$, close to the nematic domain width in this compound. Hence, similar to organic superconductors, in FeSe and other iron-based high- T_c superconductors the large size of SC domains reduces the SC enhancement by critical fluctuations. This observation may give a hint how to raise the transition temperature in high- T_c superconductors, which are always spatially inhomogeneous. The knowledge of the parameters of SC domains also helps to estimate and even to propose a possible methods of increasing the upper critical field and critical current in such heterogeneous superconductors, considered as a network of SC nanoclusters linked by Josephson junctions [68,71].

To summarize, we have shown that the scenario, in which the first-order phase transition results to spatial phase separation of SC and spin-density wave in organic superconductors, is self-consistent and also agrees with the available experimental data. We estimated the size of SC domains d by two different methods. This estimate $d > 1 \mu\text{m}$ is consistent with various transport measurements, including the anisotropic zero resistance onset in thin samples [20,21,28] and with angular magnetoresistance oscillations and magnetic-field-induced spin-density waves [21,30]. We also discuss the relevance of our results, obtained for organic superconductors, to high- T_c superconductors, and why the knowledge of SC domain parameters is important for increasing the transition temperature, the critical magnetic field H_{c2} and the critical current density in various heterogeneous superconductors.

Author Contributions: Conceptualization, P.D.G.; methodology, P.D.G. and V.D.K.; software, V.D.K.; validation, V.D.K. and S.S.S.; formal analysis, V.D.K.; investigation, V.D.K. and P.D.G.; writing—original draft preparation, V.D.K.; writing—review and editing, P.D.G. and S.S.S.; supervision, P.D.G. All authors have read and agreed to the published version of the manuscript.

Funding: V.D.K. acknowledges the Foundation for the Advancement of Theoretical Physics and Mathematics “Basis” for grant # 22-1-1-24-1, and the RFBR grant # 21-52-12027. The work of S.S.S. was support from the NUST “MISIS” grant No. K2-2022-025 in the framework of the federal academic leadership program Priority 2030. P.D.G. acknowledges the State assignment # 0033-2019-0001 and the RFBR grant # 21-52-12043.

Conflicts of Interest: The authors declare no conflict of interest.

Appendix A Mean-field theory for density wave

The electronic Hamiltonian consists of the free-electron part H_0 and the interaction part H_{int} :

$$\begin{aligned} H &= H_0 + H_{\text{int}}, \\ H_0 &= \sum_{\mathbf{k}} \varepsilon(\mathbf{k}) a_{\mathbf{k}}^\dagger a_{\mathbf{k}}, \\ H_{\text{int}} &= \frac{1}{2} \sum_{\mathbf{k}, \mathbf{k}', \mathbf{Q}} V_{\mathbf{Q}} a_{\mathbf{k}+\mathbf{Q}}^\dagger a_{\mathbf{k}} a_{\mathbf{k}'-\mathbf{Q}}^\dagger a_{\mathbf{k}'}. \end{aligned} \quad (\text{A1})$$

We consider the interactions at the wave vector \mathbf{Q} close to the nesting vector $\mathbf{Q}_0 = (\pm 2k_F, \pi/b, \pi/c)$. If the deviations from \mathbf{Q}_0 are small, we can approximate the interaction function as $V(\mathbf{Q}) \approx V(\mathbf{Q}_0) = U$. In the case of CDW U is the charge coupling constant, while for a SDW U denotes the spin coupling constant. Next, in the mean-field approximation, we introduce the order parameter

$$\begin{aligned} \Delta_{\mathbf{Q}} &= 2U \sum_{\mathbf{k}} g(\mathbf{k} - \mathbf{Q}, \mathbf{k}, -0), \\ g(\mathbf{k}, \mathbf{k}', \tau - \tau') &= \langle T_{\tau} a_{\mathbf{k}'}^\dagger(\tau') a_{\mathbf{k}}(\tau) \rangle. \end{aligned} \quad (\text{A2})$$

Then the final mean-field Hamiltonian, which we will study further, is

$$H_{\text{int}} = \sum_{\mathbf{k}, \mathbf{Q}} \Delta_{\mathbf{Q}} a_{\mathbf{k}+\mathbf{Q}}^\dagger a_{\mathbf{k}} + \text{H. c.} + \text{const.} \quad (\text{A3})$$

The factor 2 in Eqs. (A2) and (A7) comes from the summation over two spin components. The operators $a_{\mathbf{k}+\mathbf{Q}}^\dagger$ and $a_{\mathbf{k}}$ correspond to the same spin component for a CDW, and to different spin components for a SDW. From Eqs. (A1) and (A3), using the standard equation for the operator evolution $i\hbar d\hat{A}/dt = [\hat{A}, \hat{H}]$, one obtains the equations of motion for the Fourier transform of the Green’s function $g(\mathbf{k}, \mathbf{k}', \tau - \tau') = \int d\omega / (2\pi) e^{i\omega(\tau - \tau')} g(\mathbf{k}', \mathbf{k}, \omega)$:

$$[i\omega - \varepsilon(\mathbf{k})]g(\mathbf{k}', \mathbf{k}, \omega) - \sum_{\mathbf{Q}} \Delta_{\mathbf{Q}} g(\mathbf{k}', \mathbf{k}, \omega) = \delta_{\mathbf{k}', \mathbf{k}}. \quad (\text{A4})$$

In the metallic phase $\Delta_{\mathbf{Q}}$, given by Eq. (A2), vanishes after the thermodynamic averaging denoted by triangular brackets in Eq. (A2). If the DW at wave vector \mathbf{Q}_0 is formed, the order parameter $\Delta_{\mathbf{Q}} \neq 0$ for $\mathbf{Q} = \mathbf{Q}_0$, while for $\mathbf{Q} \neq \mathbf{Q}_0$ the average $\Delta_{\mathbf{Q}} = 0$. The spatial variation of the order parameter $\Delta(\mathbf{r}) = \int d^3\mathbf{q} / (2\pi) \Delta(\mathbf{q}) e^{i\mathbf{q} \cdot \mathbf{r}}$ is described by the deviation $\mathbf{q} = \mathbf{Q} - \mathbf{Q}_0$ of the DW wave vector \mathbf{Q} from its value \mathbf{Q}_0 , corresponding to the maximum of susceptibility. If we now set $\Delta_{\mathbf{Q}_1} = \Delta_{\delta\mathbf{Q}_1, \pm\mathbf{Q}}$, where $\mathbf{Q} = \mathbf{Q}_0 + \mathbf{q}$ with $|\mathbf{q}| \ll k_F$, the equations of motion (A4) can be solved giving

$$g(\mathbf{k} - \mathbf{Q}, \mathbf{k}, \omega) = -\frac{\Delta_{\mathbf{Q}}}{(\omega + i\varepsilon_+)^2 + \varepsilon_-^2 + |\Delta_{\mathbf{Q}}|^2}, \quad (\text{A5})$$

where $\varepsilon_{\pm} = \varepsilon^{\pm}(\mathbf{k}, \mathbf{k} - \mathbf{Q})$ are given by Eq. (4). From Eqs. (A2) and (A5) we obtain the self-consistency equation (7), omitting the subscript \mathbf{Q} in $\Delta_{\mathbf{Q}}$:

$$\Delta = -TU \sum_{\mathbf{k}, \omega} \frac{\Delta}{(\omega + i\varepsilon_+)^2 + \varepsilon_-^2 + |\Delta|^2}. \quad (\text{A6})$$

The mean-field Hamiltonian given by Eqs. (A1) and (A3) decouples to a sum over k of 2×2 matrices. Their diagonalization gives the new quasiparticle dispersion given by Eq. (3). Hence, the order parameter Δ_Q defined in Eq. (A2) has the physical meaning of the DW energy gap for the case of perfect nesting. One could define the order parameter in a different way as

$$n_Q = \frac{\Delta_Q}{U} = 2 \sum_k \langle T_\tau a_{k'}^\dagger(\tau') a_k(\tau) \rangle, \quad (\text{A7})$$

which has the physical meaning of electron density n_Q at wave vector Q . The latter couples to the external potential V_Q at the same wave vector in the Hamiltonian: $\delta H = \delta F = -\sum_Q n_Q V_Q$. The equilibrium value of DW order parameter $\Delta_Q = U n_Q$ in the presence of external field V_Q can be obtained from the minimization of the total free energy $F_{tot} = F + \delta F$, where the free energy F without external field is given by Eq. (5) at $\Delta_Q \rightarrow 0$:

$$\frac{\partial F_{tot}}{\partial n_Q} = -V_Q + U \frac{\partial F}{\partial \Delta_Q} = 0, \quad (\text{A8})$$

or

$$-V_Q + U^2 n_Q [A(T, Q) + B|\Delta_Q|^2 + \dots] = 0. \quad (\text{A9})$$

Hence, the electronic susceptibility just above the DW phase transition temperature T_{cDW} , where $\Delta_Q = 0$, is related to the coefficient $A(T, Q) > 0$ of the Landau-Ginzburg expansion:

$$\chi(Q) = \frac{n_Q}{V_Q} = \frac{1}{A(T, Q)U^2}. \quad (\text{A10})$$

At the DW transition temperature $T = T_{cDW}$ the coefficient $A(T, Q) = 0$ for some Q . Hence, the DW wave vector Q corresponds to the minimum of $A(T_{cDW}, Q)$ or to the maximum of susceptibility $\chi(Q)$ in Eq. (A10). Near this extremum one can expand Eq. (A10) over the deviation $q = Q - Q_0$ of the DW wave vector Q from its optimal value Q_0 :

$$\chi(Q) = \frac{\chi(Q_0)}{1 + \xi^2 q^2}, \quad (\text{A11})$$

which gives the estimate of the DW coherence length ξ .

Below the phase transition temperature T_{cDW} Eq. (A9) gives

$$\chi^{-1}(Q) = U^2 [A(T, Q) + B|\Delta|^2 + C|\Delta|^4 + \dots] \rightarrow \infty, \quad (\text{A12})$$

which corresponds to a finite Δ_Q at vanishing V_Q . Nevertheless, one can find the differential susceptibility

$$\chi^{-1}(Q) = \frac{dV_Q}{dn_Q} = \frac{\partial^2 F}{\partial n_Q^2} = U^2 \frac{\partial^2 F}{\partial \Delta_Q^2}, \quad (\text{A13})$$

which generalizes Eq. (A10).

References

1. Gabovich, A.M.; Voitenko, A.I.; Annett, J.F.; Ausloos, M. Charge- and spin-density-wave superconductors. *Supercond. Sci. Technol.* **2001**, *14*, R1–R27. <https://doi.org/10.1088/0953-2048/14/4/201>.
2. Gabovich, A.M.; Voitenko, A.I.; Ausloos, M. Charge- and spin-density waves in existing superconductors: Competition between Cooper pairing and Peierls or excitonic instabilities. *Phys. Rep.* **2002**, *367*, 583–709. [https://doi.org/10.1016/s0370-1573\(02\)00029-7](https://doi.org/10.1016/s0370-1573(02)00029-7).
3. Monceau, P. Electronic crystals: An experimental overview. *Adv. Phys.* **2012**, *61*, 325–581. <https://doi.org/10.1080/00018732.2012.719674>.
4. Grüner, G. *Density Waves in Solids*; Addison-Wesley Pub. Co., Advanced Book Program, 1994; p. 259.
5. Chang, J.; Blackburn, E.; Holmes, A.; Christensen, N.; Larsen, J.; Mesot, J.; Liang, R.; Bonn, D.; Hardy, W.; Watenphul, A.; et al. Direct observation of competition between superconductivity and charge density wave order in YBa2Cu3O6.67. *Nature Phys.* **2012**, *8*, 871–876. <https://doi.org/10.1038/nphys2456>.
6. Blanco-Canosa, S.; Frano, A.; Loew, T.; Lu, Y.; Porras, J.; Ghiringhelli, G.; Minola, M.; Mazzoli, C.; Braicovich, L.; Schierle, E.; et al. Momentum-Dependent Charge Correlations in YBa2Cu3O6+ δ Superconductors Probed by Resonant X-Ray Scattering: Evidence for Three Competing Phases. *Phys. Rev. Lett.* **2013**, *110*, 187001. <https://doi.org/10.1103/physrevlett.110.187001>.

7. Tabis, W.; Yu, B.; Bialo, I.; Bluschke, M.; Kolodziej, T.; Kozłowski, A.; Blackburn, E.; Sen, K.; Forgan, E.; Zimmermann, M.; et al. Synchrotron x-ray scattering study of charge-density-wave order in $\text{HgBa}_2\text{CuO}_{4+\delta}$. *Phys. Rev. B* **2017**, *96*, 134510. <https://doi.org/10.1103/physrevb.96.134510>.
8. Tabis, W.; Li, Y.; Tacon, M.L.; Braicovich, L.; Kreyssig, A.; Minola, M.; Dellea, G.; Weschke, E.; Veit, M.J.; Ramazanoglu, M.; et al. Charge order and its connection with Fermi-liquid charge transport in a pristine high-Tc cuprate. *Nature Communications* **2014**, *5*, 5875. <https://doi.org/10.1038/ncomms6875>.
9. da Silva Neto, E.H.; Comin, R.; He, F.; Sutarto, R.; Jiang, Y.; Greene, R.L.; Sawatzky, G.A.; Damascelli, A. Charge ordering in the electron-doped superconductor $\text{Nd}_{2-x}\text{Ce}_x\text{CuO}_4$. *Science* **2015**, *347*, 282–285, [<https://www.science.org/doi/pdf/10.1126/science.1256441>]. <https://doi.org/10.1126/science.1256441>.
10. Wen, J.J.; Huang, H.; Lee, S.J.; Jang, H.; Knight, J.; Lee, Y.S.; Fujita, M.; Suzuki, K.M.; Asano, S.; Kivelson, S.A.; et al. Observation of two types of charge-density-wave orders in superconducting $\text{La}_{2-x}\text{Sr}_x\text{CuO}_4$. *Nature Communications* **2019**, *10*, 3269. <https://doi.org/10.1038/s41467-019-11167-z>.
11. Si, Q.; Yu, R.; Abrahams, E. High-temperature superconductivity in iron pnictides and chalcogenides. *Nat Rev Mater* **2016**, *1*, 16017. <https://doi.org/10.1038/natrevmats.2016.17>.
12. Liu, X.; Zhao, L.; He, S.; He, J.; Liu, D.; Mou, D.; Shen, B.; Hu, Y.; Huang, J.; Zhou, X.J. Electronic structure and superconductivity of FeSe-related superconductors. *J. Phys.: Condens. Matter* **2015**, *27*, 183201. <https://doi.org/10.1088/0953-8984/27/18/183201>.
13. Ishiguro, T.; Yamaji, K.; Saito, G. *Organic Superconductors*; Springer Berlin Heidelberg, 1998. <https://doi.org/10.1007/978-3-642-58262-2>.
14. Lebed, A., Ed. *The Physics of Organic Superconductors and Conductors*; Springer Berlin Heidelberg, 2008. <https://doi.org/10.1007/978-3-540-76672-8>.
15. Naito, T. Modern History of Organic Conductors: An Overview. *Crystals* **2021**, *11*. <https://doi.org/10.3390/cryst11070838>.
16. Yasuzuka, S.; Murata, K. Recent progress in high-pressure studies on organic conductors. *Science and Technology of Advanced Materials* **2009**, *10*, 024307, [<https://doi.org/10.1088/1468-6996/10/2/024307>]. <https://doi.org/10.1088/1468-6996/10/2/024307>.
17. Clay, R.; Mazumdar, S. From charge- and spin-ordering to superconductivity in the organic charge-transfer solids. *Physics Reports* **2019**, *788*, 1–89. From charge- and spin-ordering to superconductivity in the organic charge-transfer solids, <https://doi.org/https://doi.org/10.1016/j.physrep.2018.10.006>.
18. Lee, I.J.; Chaikin, P.M.; Naughton, M.J. Critical Field Enhancement near a Superconductor-Insulator Transition. *Phys. Rev. Lett.* **2002**, *88*, 207002. <https://doi.org/10.1103/physrevlett.88.207002>.
19. Vuletić, T.; Auban-Senzier, P.; Pasquier, C.; Tomić, S.; Jérôme, D.; Héritier, M.; Bechgaard, K. Coexistence of superconductivity and spin density wave orderings in the organic superconductor $\text{TMTSF}(2\text{PF}_6)$. *Eur. Phys. J. B* **2002**, *25*, 319–331. <https://doi.org/10.1140/epjb/e20020037>.
20. Kang, N.; Salameh, B.; Auban-Senzier, P.; Jerome, D.; Pasquier, C.R.; Brazovskii, S. Domain walls at the spin-density-wave endpoint of the organic superconductor $\text{TMTSF}(2\text{PF}_6)$ under pressure. *Phys. Rev. B* **2010**, *81*, 100509(R). <https://doi.org/10.1103/physrevb.81.100509>.
21. Narayanan, A.; Kiswandhi, A.; Graf, D.; Brooks, J.; Chaikin, P. Coexistence of Spin Density Waves and Superconductivity in $\text{TMTSF}(2\text{PF}_6)$. *Phys. Rev. Lett.* **2014**, *112*, 146402. <https://doi.org/10.1103/physrevlett.112.146402>.
22. Lee, I.J.; Brown, S.E.; Yu, W.; Naughton, M.J.; Chaikin, P.M. Coexistence of Superconductivity and Antiferromagnetism Probed by Simultaneous Nuclear Magnetic Resonance and Electrical Transport in $\text{TMTSF}(2\text{PF}_6)$ System. *Phys. Rev. Lett.* **2005**, *94*, 197001. <https://doi.org/10.1103/physrevlett.94.197001>.
23. Lee, I.J.; Naughton, M.J.; Danner, G.M.; Chaikin, P.M. Anisotropy of the Upper Critical Field in $\text{TMTSF}(2\text{PF}_6)$. *Phys. Rev. Lett.* **1997**, *78*, 3555–3558. <https://doi.org/10.1103/physrevlett.78.3555>.
24. Lee, I.J.; Brown, S.E.; Clark, W.G.; Strouse, M.J.; Naughton, M.J.; Kang, W.; Chaikin, P.M. Triplet Superconductivity in an Organic Superconductor Probed by NMR Knight Shift. *Phys. Rev. Lett.* **2001**, *88*, 017004. <https://doi.org/10.1103/physrevlett.88.017004>.
25. Andres, D.; Kartsovnik, M.V.; Biberacher, W.; Neumaier, K.; Schuberth, E.; Muller, H. Superconductivity in the charge-density-wave state of the organic metal $\alpha-(\text{BEDT}-\text{TTF})_2\text{KHg}(\text{SCN})_4$. *Phys. Rev. B* **2005**, *72*, 174513. <https://doi.org/10.1103/physrevb.72.174513>.
26. Itoi, M.; Nakamura, T.; Uwatoko, Y. Pressure-Induced Superconductivity of the Quasi-One-Dimensional Organic Conductor $\text{TMTTF}(2\text{TaF}_6)$. *Materials* **2022**, *15*. <https://doi.org/10.3390/ma15134638>.
27. Cho, K.; Kończykowski, M.; Teknowijoyo, S.; Tanatar, M.; Guss, J.; Gartin, P.; Wilde, J.; Kreyssig, A.; McQueeney, R.; Goldman, A.; et al. Using controlled disorder to probe the interplay between charge order and superconductivity in NbSe_2 . *Nat Commun* **2018**, *9*, 2796. <https://doi.org/10.1038/s41467-018-05153-0>.
28. Gerasimenko, Y.A.; Sanduleanu, S.V.; Prudkoglyad, V.A.; Kornilov, A.V.; Yamada, J.; Qualls, J.S.; Pudalov, V.M. Coexistence of superconductivity and spin-density wave in $\text{TMTSF}(2\text{ClO}_4)$: Spatial structure of the two-phase state. *Phys. Rev. B* **2014**, *89*, 054518. <https://doi.org/10.1103/physrevb.89.054518>.
29. Yonezawa, S.; Marrache-Kikuchi, C.A.; Bechgaard, K.; Jerome, D. Crossover from impurity-controlled to granular superconductivity in $\text{TMTSF}(2\text{ClO}_4)$. *Phys. Rev. B* **2018**, *97*, 014521. <https://doi.org/10.1103/physrevb.97.014521>.
30. Gerasimenko, Y.A.; Prudkoglyad, V.A.; Kornilov, A.V.; Sanduleanu, S.V.; Qualls, J.S.; Pudalov, V.M. Role of anion ordering in the coexistence of spin-density-wave and superconductivity in $\text{TMTSF}(2\text{ClO}_4)$. *JETP Lett.* **2013**, *97*, 419–424. <https://doi.org/10.1134/S0021364013070060>.

31. Gabovich, A.M.; Voitenko, A.I.; Annett, J.F.; Ausloos, M. Charge- and spin-density-wave superconductors. *Superconductor Science and Technology* **2001**, *14*, R1. <https://doi.org/10.1088/0953-2048/14/4/201>.
32. Gabovich, A.; Voitenko, A.; Ausloos, M. Charge- and spin-density waves in existing superconductors: competition between Cooper pairing and Peierls or excitonic instabilities. *Physics Reports* **2002**, *367*, 583–709. [https://doi.org/10.1016/S0370-1573\(02\)00029-7](https://doi.org/10.1016/S0370-1573(02)00029-7).
33. Wang, Y.; Chubukov, A.V. Enhancement of superconductivity at the onset of charge-density-wave order in a metal. *Phys. Rev. B* **2015**, *92*, 125108. <https://doi.org/10.1103/PhysRevB.92.125108>.
34. Eckberg, C.; Campbell, D.J.; Metz, T.; Collini, J.; Hodovanets, H.; Drye, T.; Zavalij, P.; Christensen, M.H.; Fernandes, R.M.; Lee, S.; et al. Sixfold enhancement of superconductivity in a tunable electronic nematic system. *Nature Physics* **2020**, *16*, 346–350. <https://doi.org/10.1038/s41567-019-0736-9>.
35. Mukasa, K.; Ishida, K.; Imajo, S.; Qiu, M.; Saito, M.; Matsuura, K.; Sugimura, Y.; Liu, S.; Uezono, Y.; Otsuka, T.; et al. Enhanced Superconducting Pairing Strength near a Pure Nematic Quantum Critical Point. *Phys. Rev. X* **2023**, *13*, 011032. <https://doi.org/10.1103/PhysRevX.13.011032>.
36. Tanaka, Y.; Kuroki, K. Microscopic theory of spin-triplet *f*-wave pairing in quasi-one-dimensional organic superconductors. *Phys. Rev. B* **2004**, *70*, 060502. <https://doi.org/10.1103/PhysRevB.70.060502>.
37. Kartsovnik, M.V. High Magnetic Fields: A Tool for Studying Electronic Properties of Layered Organic Metals. *Chem. Rev.* **2004**, *104*, 5737–5782. <https://doi.org/10.1021/cr0306891>.
38. Grigoriev, P.D. Properties of superconductivity on a density wave background with small ungapped Fermi surface parts. *Phys. Rev. B* **2008**, *77*, 224508. <https://doi.org/10.1103/physrevb.77.224508>.
39. Brazovskii, S.; Kirova, N. Electron selflocalization and superstructures in quasi one-dimensional dielectrics. *Sov. Sci. Rev. A* **1984**, *5*, 99–166.
40. Su, W.P.; Kivelson, S.; Schrieffer, J.R. Theory of Polymers Having Broken Symmetry Ground States. In *Physics in One Dimension*; Bernasconi, J.; Schneider, T., Eds.; Springer Series in Solid-State Sciences, Springer Berlin Heidelberg, 1981; pp. 201–211. https://doi.org/10.1007/978-3-642-81592-8_22.
41. Grigoriev, P.D. Superconductivity on the density-wave background with soliton-wall structure. *Physica B* **2009**, *404*, 513–516. <https://doi.org/10.1016/j.physb.2008.11.056>.
42. Gor'kov, L.P.; Grigoriev, P.D. Soliton phase near antiferromagnetic quantum critical point in Q1D conductors. *Europhys. Lett.* **2005**, *71*, 425–430. <https://doi.org/10.1209/epl/i2005-10089-y>.
43. Gor'kov, L.P.; Grigoriev, P.D. Nature of the superconducting state in the new phase in (TMTSF)₂PF₆ under pressure. *Phys. Rev. B* **2007**, *75*, 020507(R). <https://doi.org/10.1103/physrevb.75.020507>.
44. Tinkham, M. *Introduction to superconductivity*, 2 ed.; International series in pure and applied physics, McGraw-Hill, Inc.: New York, 1996.
45. Pratt, F.L.; Lancaster, T.; Blundell, S.J.; Baines, C. Low-Field Superconducting Phase of (TMTSF)₂ClO₄. *Phys. Rev. Lett.* **2013**, *110*, 107005. <https://doi.org/10.1103/PhysRevLett.110.107005>.
46. Kochev, V.D.; Kesharpur, K.K.; Grigoriev, P.D. Anisotropic zero-resistance onset in organic superconductors. *Phys. Rev. B* **2021**, *103*, 014519. <https://doi.org/10.1103/PhysRevB.103.014519>.
47. Grigoriev, P.D.; Kochev, V.D.; Orlov, A.P.; Frolov, A.V.; Sinchenko, A.A. Inhomogeneous Superconductivity Onset in FeSe Studied by Transport Properties. *Materials* **2023**, *16*. <https://doi.org/10.3390/ma16051840>.
48. Seidov, S.S.; Kochev, V.D.; Grigoriev, P.D. First-order phase transition between superconductivity and charge/spin-density wave as the reason of their coexistence in organic metals, 2023, [arXiv:cond-mat.supr-con/2305.06957].
49. Valfells, S.; Brooks, J.S.; Wang, Z.; Takasaki, S.; Yamada, J.; Anzai, H.; Tokumoto, M. Quantum Hall transitions in (TMTSF)₂PF₆. *Phys. Rev. B* **1996**, *54*, 16413–16416. <https://doi.org/10.1103/PhysRevB.54.16413>.
50. Danner, G.M.; Chaikin, P.M.; Hannahs, S.T. Critical imperfect nesting in (TMTSF)₂PF₆. *Phys. Rev. B* **1996**, *53*, 2727–2731. <https://doi.org/10.1103/PhysRevB.53.2727>.
51. Araki, C.; Itoi, M.; Hedo, M.; Uwatoko, Y.; Mori, H. Electrical Resistivity of (TMTTF)₂PF₆ under High Pressure. *Journal of the Physical Society of Japan* **2007**, *76*, 198–199, [https://doi.org/10.1143/JPSJS.76SA.198]. <https://doi.org/10.1143/JPSJS.76SA.198>.
52. Auban-Senzier, P.; Pasquier, C.; Jérôme, D.; Carcel, C.; Fabre, J. From Mott insulator to superconductivity in (TMTTF)₂BF₄: high pressure transport measurements. *Synthetic Metals* **2003**, *133–134*, 11–14. Proceedings of the Yamada Conference LVI. The Fourth International Symposium on Crystalline Organic Metals, Superconductors and Ferromagnets (ISCOM 2001), [https://doi.org/10.1016/S0379-6779\(02\)00420-4](https://doi.org/10.1016/S0379-6779(02)00420-4).
53. Horovitz, B.; Gutfreund, H.; Weger, M. Interchain coupling and the Peierls transition in linear-chain systems. *Phys. Rev. B* **1975**, *12*, 3174–3185. <https://doi.org/10.1103/PhysRevB.12.3174>.
54. McKenzie, R.H. Microscopic theory of the pseudogap and Peierls transition in quasi-one-dimensional materials. *Phys. Rev. B* **1995**, *52*, 16428–16442. <https://doi.org/10.1103/PhysRevB.52.16428>.
55. Grigoriev, P.D.; Lyubshin, D.S. Phase diagram and structure of the charge-density-wave state in a high magnetic field in quasi-one-dimensional materials: A mean-field approach. *Phys. Rev. B* **2005**, *72*, 195106. <https://doi.org/10.1103/PhysRevB.72.195106>.
56. Kim, J.; Yun, M.; Jeong, D.W.; Kim, J.J.; Lee, I. Structural and Electrical Properties of the Single-crystal Organic Semiconductor Tetramethyltetraselenafulvalene (TMTSF). *Journal of the Korean Physical Society* **2009**, *55*, 212–216. <https://doi.org/10.3938/jkps.55.212>.

57. Oxtoby, D.W. Nucleation of First-Order Phase Transitions. *Accounts of Chemical Research* **1998**, *31*, 91–97. <https://doi.org/10.1021/ar9702278>.
58. Umantsev, A. *Field Theoretic Method in Phase Transformations*; Lecture Notes in Physics, Springer New York, 2012. <https://doi.org/10.1007/978-1-4614-1487-2>.
59. Kalikmanov, V. *Nucleation Theory*; Lecture Notes in Physics, Springer Netherlands, 2012. <https://doi.org/10.1007/978-90-481-3643-8>.
60. Karthika, S.; Radhakrishnan, T.K.; Kalaichelvi, P. A Review of Classical and Nonclassical Nucleation Theories. *Crystal Growth & Design* **2016**, *16*, 6663–6681. <https://doi.org/10.1021/acs.cgd.6b00794>.
61. Efros, A.L. *Physics and Geometry of Disorder: Percolation Theory*; Science for Everyone, Imported Pubn, 1987.
62. Torquato, S. *Random Heterogeneous Materials*; Springer New York, 2002. <https://doi.org/10.1007/978-1-4757-6355-3>.
63. Sinchenko, A.A.; Grigoriev, P.D.; Orlov, A.P.; Frolov, A.V.; Shakin, A.; Chareev, D.A.; Volkova, O.S.; Vasiliev, A.N. Gossamer high-temperature bulk superconductivity in FeSe. *Phys. Rev. B* **2017**, *95*, 165120. <https://doi.org/10.1103/physrevb.95.165120>.
64. Grigoriev, P.D.; Sinchenko, A.A.; Kesharpu, K.K.; Shakin, A.; Mogilyuk, T.I.; Orlov, A.P.; Frolov, A.V.; Lyubshin, D.S.; Chareev, D.A.; Volkova, O.S.; et al. Anisotropic effect of appearing superconductivity on the electron transport in FeSe. *JETP Lett.* **2017**, *105*, 786–791. <https://doi.org/10.1134/s0021364017120074>.
65. Seidov, S.S.; Kesharpu, K.K.; Karpov, P.I.; Grigoriev, P.D. Conductivity of anisotropic inhomogeneous superconductors above the critical temperature. *Phys. Rev. B* **2018**, *98*, 014515. <https://doi.org/10.1103/physrevb.98.014515>.
66. Lang, K.M.; Madhavan, V.; Hoffman, J.E.; Hudson, E.W.; Eisaki, H.; Uchida, S.; Davis, J.C. Imaging the granular structure of high-Tc superconductivity in underdoped Bi₂Sr₂CaCu₂O_{8+δ}. *Nature* **2002**, *415*, 412–416. <https://doi.org/10.1038/415412a>.
67. Wise, W.D.; Chatterjee, K.; Boyer, M.C.; Kondo, T.; Takeuchi, T.; Ikuta, H.; Xu, Z.; Wen, J.; Gu, G.D.; Wang, Y.; et al. Imaging nanoscale Fermi-surface variations in an inhomogeneous superconductor. *Nature Phys* **2009**, *5*, 213–216. <https://doi.org/10.1038/nphys1197>.
68. Kresin, V.; Ovchinnikov, Y.; Wolf, S. Inhomogeneous superconductivity and the “pseudogap” state of novel superconductors. *Phys. Rep.* **2006**, *431*, 231–259. <https://doi.org/10.1016/j.physrep.2006.05.006>.
69. Campi, G.; Bianconi, A.; Poccia, N.; Bianconi, G.; Barba, L.; Arrighetti, G.; Innocenti, D.; Karpinski, J.; Zhigadlo, N.D.; Kazakov, S.M.; et al. Inhomogeneity of charge-density-wave order and quenched disorder in a high-Tc superconductor. *Nature* **2015**, *525*, 359–362. <https://doi.org/10.1038/nature14987>.
70. Mogilyuk, T.I.; Grigoriev, P.D.; Kesharpu, K.K.; Kolesnikov, I.A.; Sinchenko, A.A.; Frolov, A.V.; Orlov, A.P. Excess Conductivity of Anisotropic Inhomogeneous Superconductors Above the Critical Temperature. *Physics of the Solid State* **2019**, *61*, 1549–1552. <https://doi.org/10.1134/S1063783419090166>.
71. Kresin, V.Z.; Ovchinnikov, Y.N. Nano-based Josephson Tunneling Networks and High Temperature Superconductivity. *Journal of Superconductivity and Novel Magnetism* **2021**, *34*, 1705–1708. <https://doi.org/10.1007/s10948-020-05768-9>.